Exotic nuclei and drip lines

- Unstable vs. stable nuclei: neutron-rich and proton-rich (or neutron-deficient) systems
- Limit of nuclear stability and definition of drip lines
- Discovering new isotopes
- Radioactive beam facilities
- Measurements of masses and sizes of exotic nuclei
- Halo nuclei

The Karlsruhe Nuclide Chart

A nuclide chart is a two dimensional representation of the nuclear and radioactive properties of all known atoms. A nuclide is the generic name for atoms characterized by the constituent protons and neutrons. The nuclide chart arranges nuclides according to the number of protons (vertical axis) and neutrons (horizontal axis) in the nucleus. Each nuclide in the chart is represented by a box containing the element symbol and mass number, half-life, decay types and decay energies, etc.

"Magic" numbers

In nuclear physics, a magic number is a number of protons or neutrons (e.g. 2, 8, 20, 28, 50, 82, 126) which give rise to a complete shell in the atomic nucleus. Lead 208 for example, which consists of 82 protons and 126 neutrons, is called "doubly magic" since both the proton and neutron numbers are "magic".

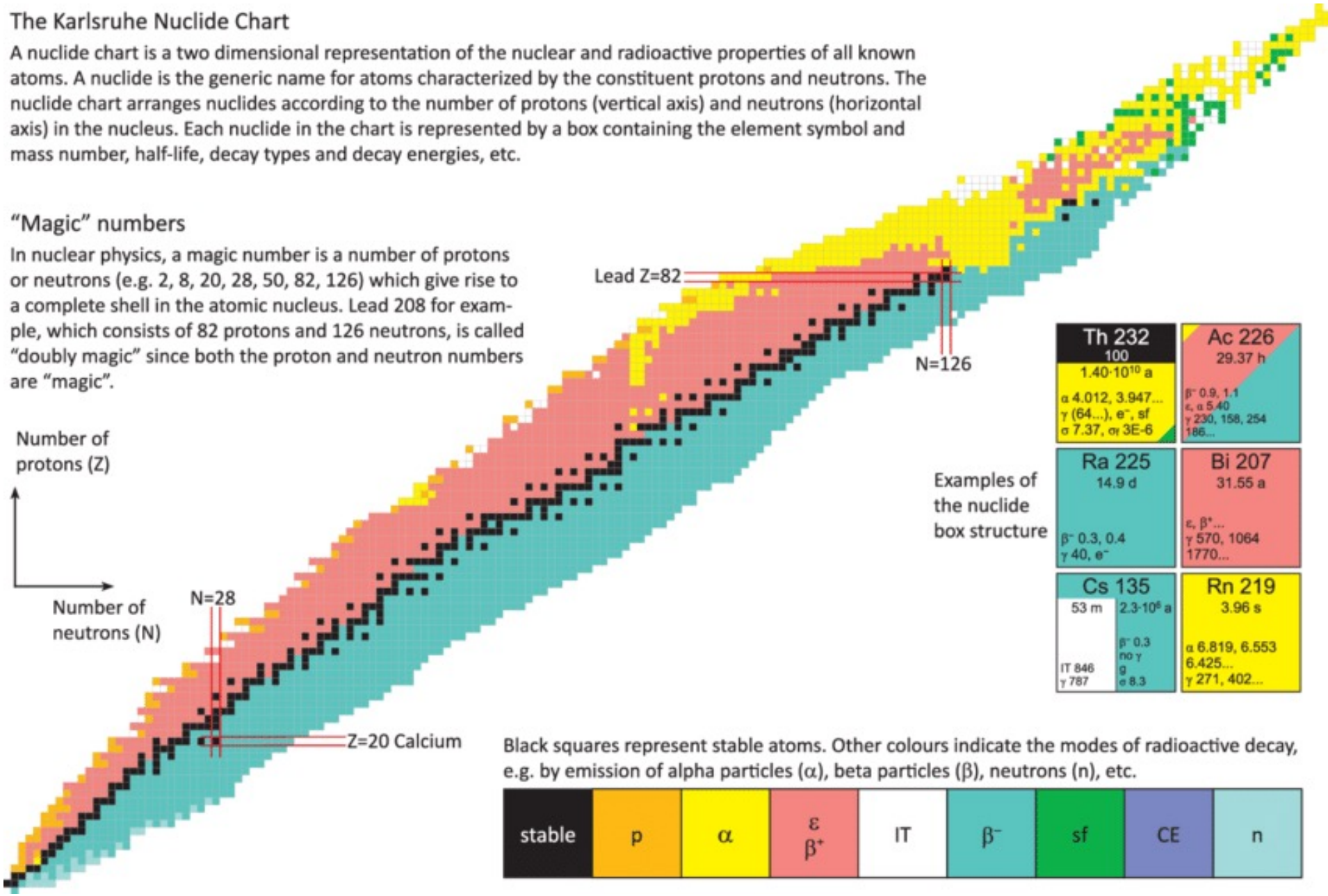

Black squares represent stable atoms. Other colours indicate the modes of radioactive decay, e.g. by emission of alpha particles (α), beta particles (β), neutrons (n), etc.

stable	p	α	ε β⁺	IT	β⁻	sf	CE	n

Cite this article as: Zsolt Sóti, Joseph Magill, Raymond Dreher, Karlsruhe Nuclide Chart – New 10th edition 2018 , EPJ Nuclear Sci. Technol. **5**, 6 (2019)

Let us focus on Z=50 (Sn isotopes)

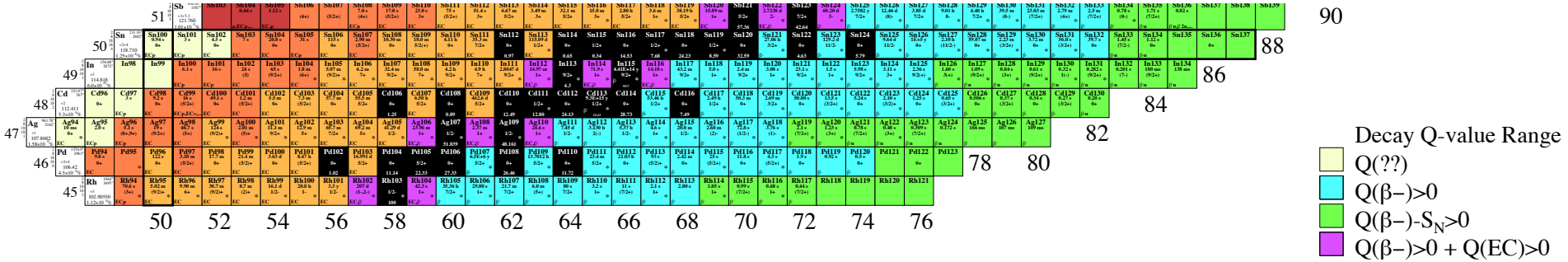

From the above figure we can see that even-even systems are stable, and naturally abundant, in the range A = 112-124.

If they have more neutrons, they undergo β^- decay.

If they have less neutrons, they undergo β^+ decay.

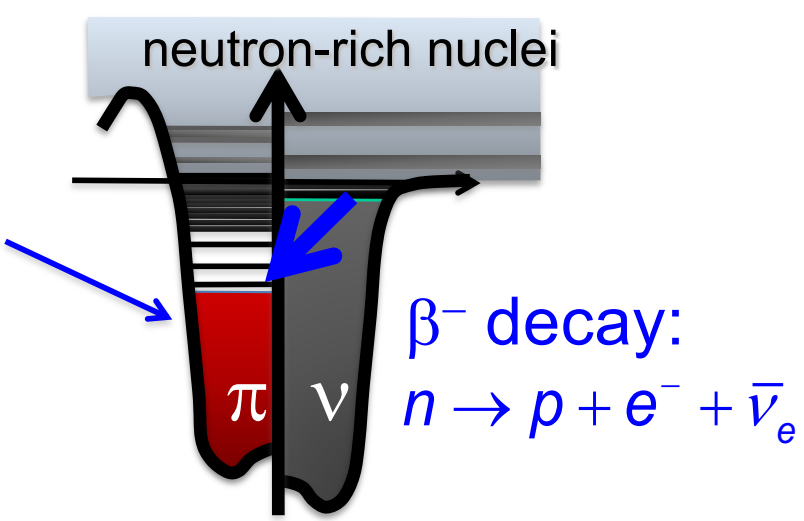

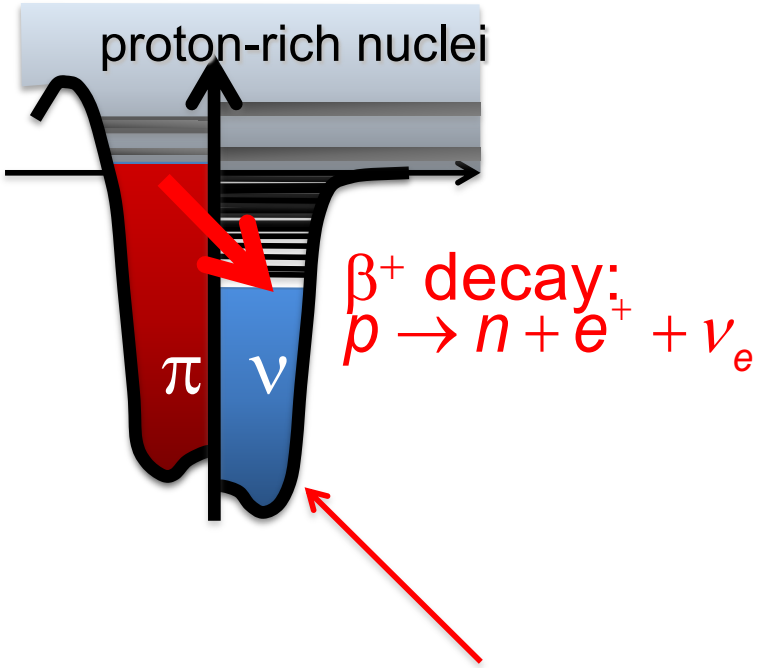

- Nuclei that are neutron-rich or proton-deficient undergo β-decay.

- Although unstable, these nuclei exist as bound systems. The limit of nuclear stability with respect to the strong interaction is the **drip line**. Neutron and proton **drip lines** are **only partially known.**

Neutron-rich and proton rich nuclei in HF with effective forces:

Reminder: the pp and nn force is active only in the T=1 channel (on average, not so much attractive), whereas the pn force is active also in the T=0 channel which provides stronger attraction. This is known from the existence of the deuteron as a bound system, and the non-existence of the di-neutron.

Therefore, neutrons feel more the proton attraction than the attraction of the other neutrons. In a system with increasing N-Z, the neutrons become much less bound with respect to the protons.

For analogous reasons, in a system which is neutron deficient, the protons become much less bound with respect to the neutrons.

Gamow-Teller beta decay and isospin impurity in nuclei near the proton drip line

I. Hamamoto[1,2] and H. Sagawa[1,3]
[1]*Department of Physics, Faculty of Science, The University of Tokyo, Hongo 7-3-1, Bunkyo-ku, Tokyo 113, Japan*
[2]*Department of Mathematical Physics, Lund Institute of Technology, Lund, Sweden**
[3]*Center for Mathematical Sciences, University of Aizu, Aizu-Wakamatsu, Fukushima 965, Japan**
(Received 4 May 1993)

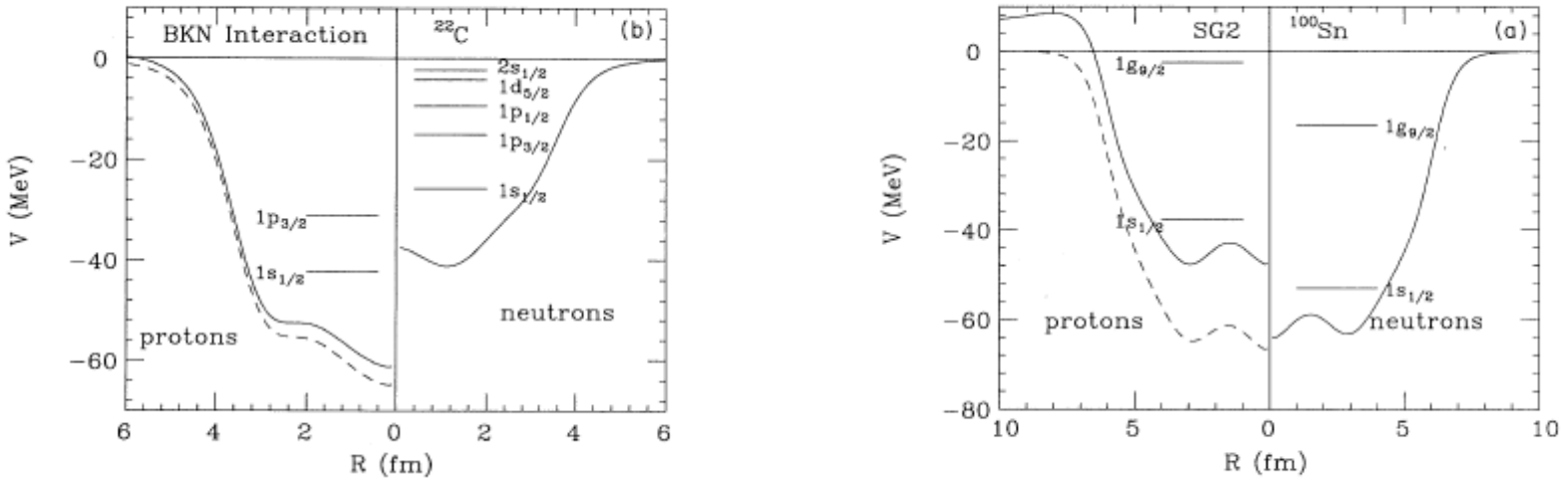

FIG. 1. HF potentials of ^{100}Sn (a) and ^{22}C (b). The Skyrme interactions, SG2 and BKN, are used for ^{100}Sn and ^{22}C, respectively. The dashed (solid) lines for protons show the HF potential without (with) the Coulomb potential. Since the HF calculation is performed with the Coulomb potential, there is a small difference between the dashed line for protons and the solid line for neutrons in ^{100}Sn. In ^{100}Sn only the lowest-lying one-particle level ($=1s_{1/2}$) and the highest occupied level ($=1g_{9/2}$) are shown, while in ^{22}C all occupied one-particle levels are denoted.

Lifetimes for beta-decay can be quite short – and yet, unstable nuclei can nonetheless be studied **nowadays** using RIB (Radioactive Isotope Beam) facilities.

We meet, by further increasing (or decreasing) N-Z, the neutron (proton) drip line. **These are defined as the limits beyond which the systems are unstable against particle emission.** In the case of neutrons, the one-neutron or two-neutron separation energies (S_n = BE(N)-BE(N-1) or S_{2n}) become zero.

In certain cases, systems beyond the drip lines can be studied: for instance, if the lifetime is relatively long, due to the fact that the extra neutron (or proton) has a resonant state available. But this is not the rule !

Theoretical predictions of the drip lines

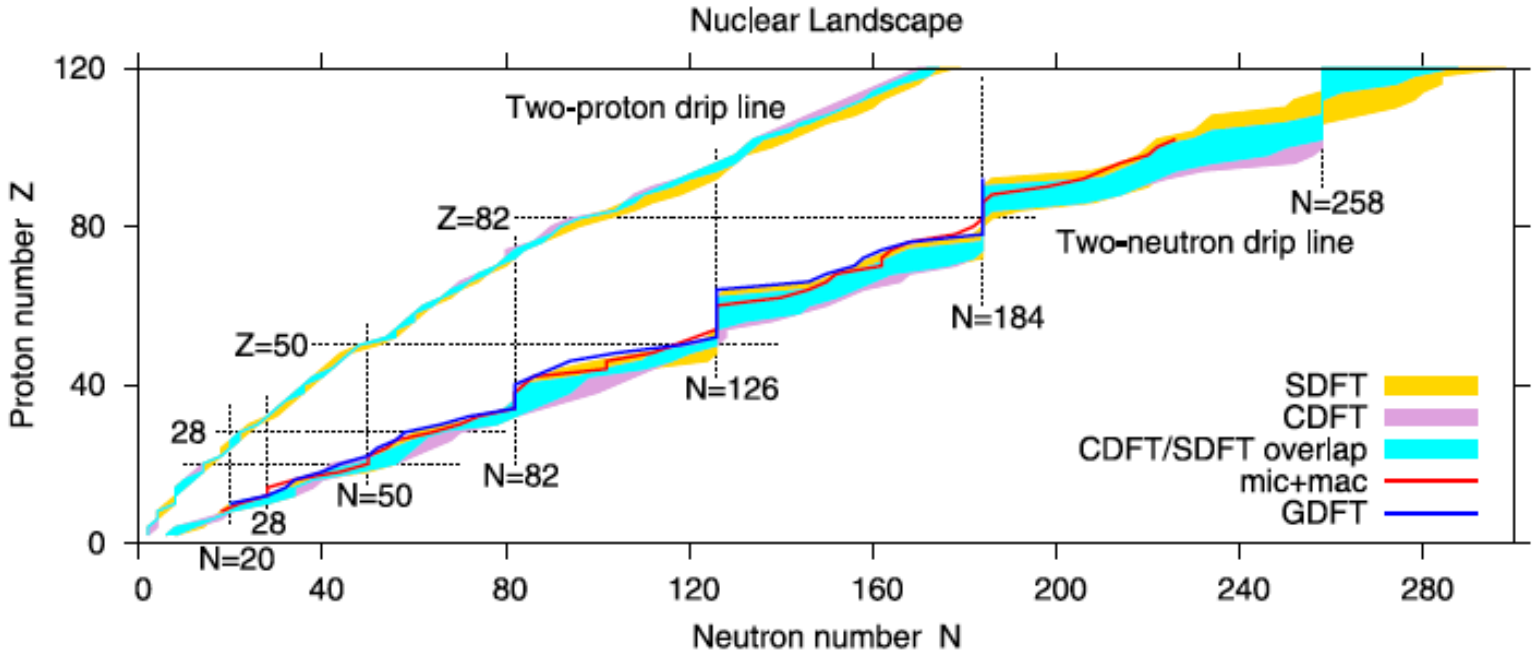

Fig. 4. The comparison of the uncertainties in the definition of two-proton and two-neutron drip lines obtained in CDFT and SDFT. The shaded areas are defined by the extremes of the predictions of the corresponding drip lines obtained with different parametrizations. The blue shaded area shows the area where the CDFT and SDFT results overlap. Non-overlapping regions are shown by dark yellow and plum colors for SDFT and CDFT, respectively. The results of the SDFT calculations are taken from the supplement to Ref. [2]. The two-neutron drip lines obtained by microscopic + macroscopic (FRDM [3]) and Gogny D1S DFT [5] calculations are shown by red and blue lines, respectively. (For interpretation of the references to color in this figure legend, the reader is referred to the web version of this Letter.)

A.V. Afanasjev *et al.*, Phys. Lett. B726, 680 (2013) - CEDF

J. Erler *et al.*, Nature 486, 509 (2012) - SEDF

PHYSICAL REVIEW LETTERS **126,** 022501 (2021)

Editors' Suggestion | Featured in Physics

Ab Initio Limits of Atomic Nuclei

S. R. Stroberg,[1,2,*] J. D. Holt,[2,3,†] A. Schwenk,[4,5,6,‡] and J. Simonis[7,4,5,§]

[1]*Department of Physics, University of Washington, Seattle, Washington 98195, USA*
[2]*TRIUMF, 4004 Wesbrook Mall, Vancouver, British Columbia V6T 2A3, Canada*
[3]*Department of Physics, McGill University, 3600 Rue University, Montréal, Quebec H3A 2T8, Canada*
[4]*Institut für Kernphysik, Technische Universität Darmstadt, 64289 Darmstadt, Germany*
[5]*ExtreMe Matter Institute EMMI, GSI Helmholtzzentrum für Schwerionenforschung GmbH, 64291 Darmstadt, Germany*
[6]*Max-Planck-Institut für Kernphysik, Saupfercheckweg 1, 69117 Heidelberg, Germany*
[7]*Institut für Kernphysik and PRISMA Cluster of Excellence, Johannes Gutenberg-Universität, 55099 Mainz, Germany*

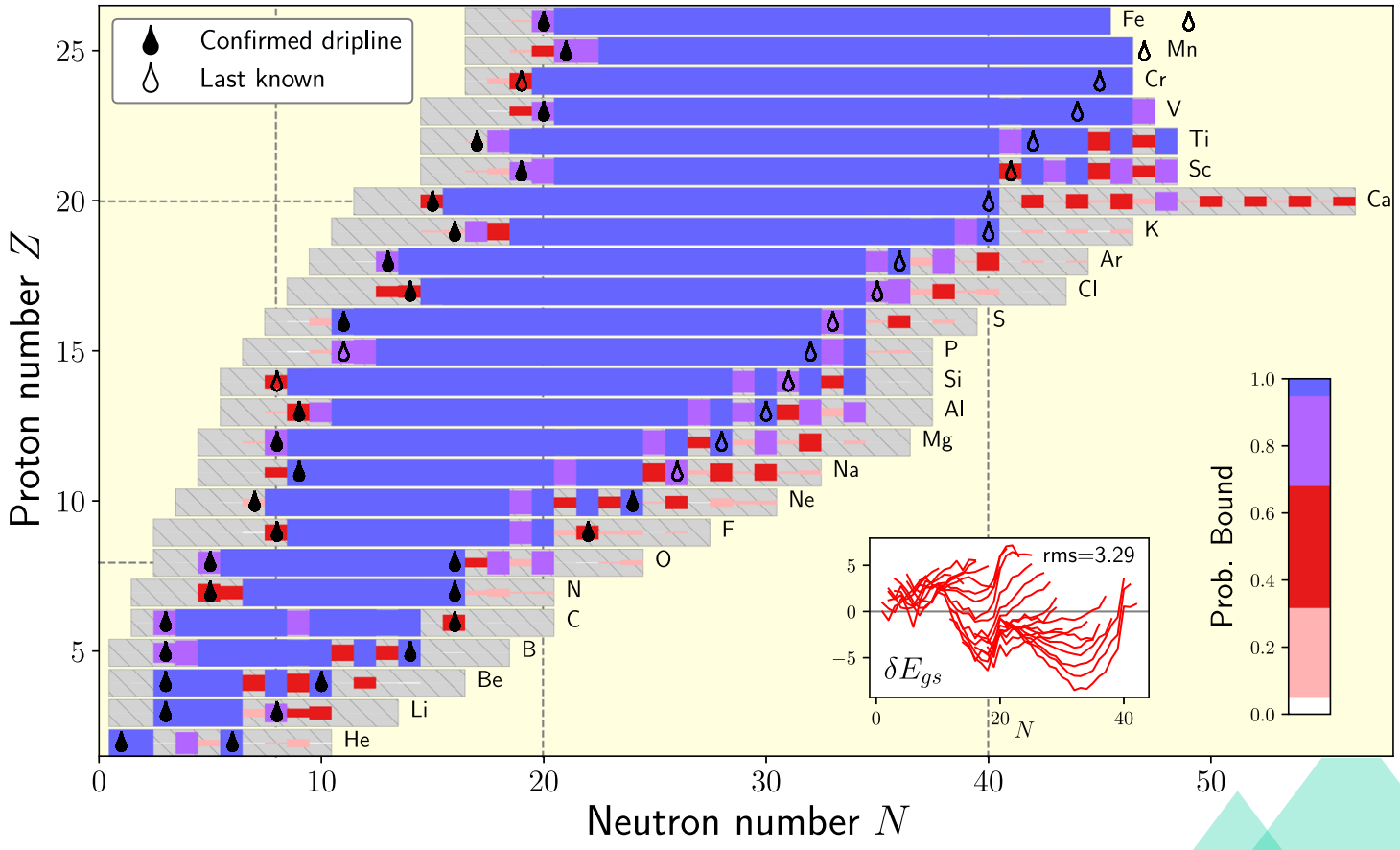

Simple estimates (for mere pedagogical purposes) can be done using the mass formula.

First problems:

- For each value of A (i.e., for each isobaric chain), which is the nucleus with largest binding energy ?
- How does this evolve if we move towards right (left) in the previous figure, that is, if we move by increasing (decreasing) (N-Z) ?
- How are the parameters of the mass formula sensitive to the drip lines ?

The solution of the first problem can be attempted by using the well-known Bethe-Weiszäcker mass formula. We take this problem from [Hey94].

$$
\begin{aligned}
& M(A,Z)c^2 = Zm_pc^2 + (A-Z)m_nc^2 \\
& -a_V A + a_S A^{2/3} + a_A(A-2Z)^2A^{-1} \\
& +a_C Z(Z-1)A^{-1/3} + \\
& \text{pairing term} : 0, \pm\delta. \qquad (1)
\end{aligned}
$$

If we wish, for each A, the nucleus with the lowest mass, or largest binding energy, we must re-write the above equation (neglecting the pairing term) as

$$M(A,Z)c^2 = f(A) + pZ + qZ^2, \qquad (2)$$

where the constants p and q can be easily obtained, and then

$$\frac{\partial}{\partial Z}Mc^2 = 0 \qquad (3)$$

is solved for

$$Z_0 = \frac{-p}{2q}. \qquad (4)$$

We can obtain Z_0 (value of Z corresponding to the lowest mass) by replacing the values of p and q and then multiplying the numerator and denominator by $A/8a_A$:

$$Z_0 = \frac{\frac{A}{2} + (m_n - m_p)c^2\frac{A}{8a_A} + \frac{a_C A^{2/3}}{8a_A}}{1 + \frac{1}{4}\frac{a_C}{a_A}A^{2/3}}. \qquad (1)$$

In the numerator, the second and third terms are negligible with respect to the first one. This leads to

$$Z_0 = \frac{\frac{A}{2}}{1 + 0.0077A^{2/3}}. \qquad (2)$$

Values:

a_V=15.85 MeV
a_S=18.34 MeV
a_C=0.71 MeV
a_A=23.21 MeV

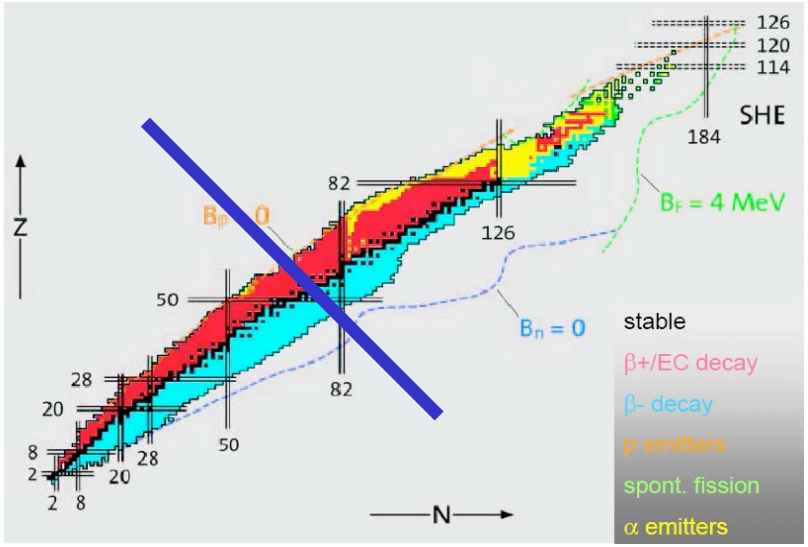

The blue line represents constant A: for A=120 we meet Z_0 close to 50 (i.e., Sn).

Discovering new isotopes

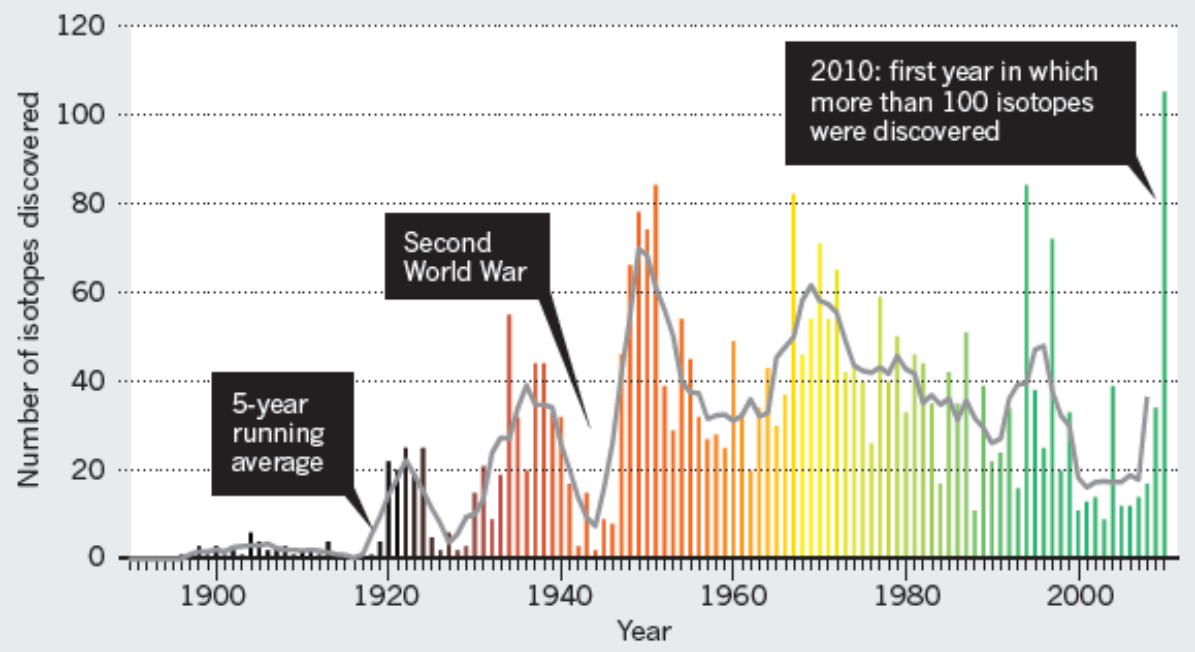

M. Thoennessen, B. Sherrill, Nature 473, 25 (2011).

https://people.nscl.msu.edu/~thoennes/isotopes/

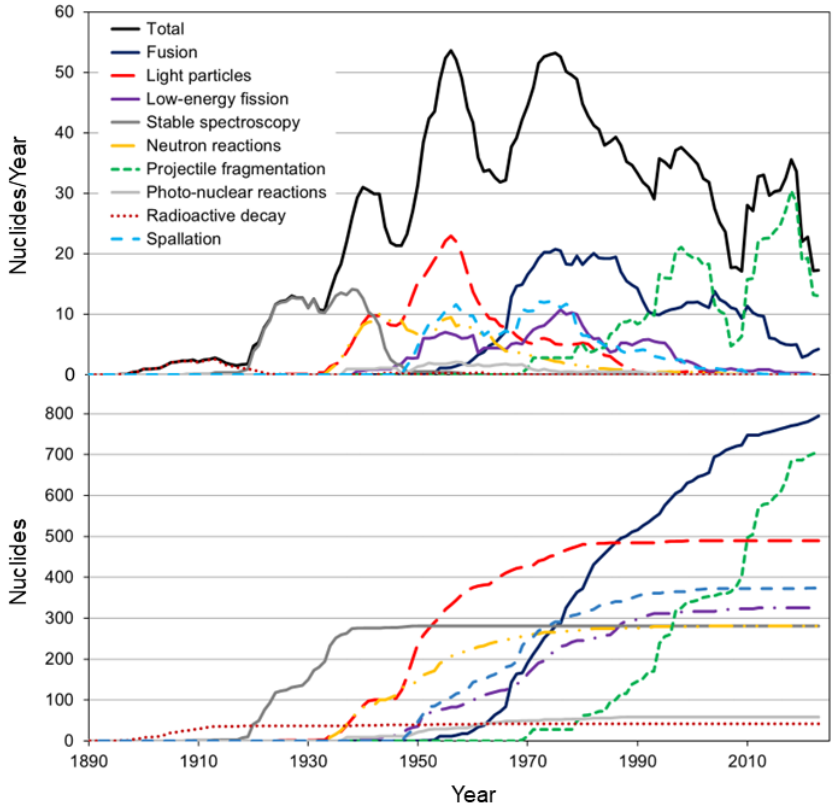

2023 update:
arXiv:2403.17750
Published in IJMPE

Table 1. New nuclides reported in 2023. The nuclides are listed with the first author, submission date, and reference of the publication, the laboratory where the experiment was performed, and the production method (PF = projectile fragmentation, FE = fusion evaporation, SB = secondary beams, TR = transfer reactions).

Nuclide(s)	First Author	Subm. Date	Ref.	Laboratory	Type
^{116}La[a]	W. Zhang	7/5/2022	13	Jyväskylä	FE
^{27}O, ^{28}O	Y. Kondo	10/13/2022	14	RIKEN	SB
^{9}N	R. J. Charity	11/2/2022	15	MSU	SB
^{241}U	T. Niwase	11/21/2022	16	RIKEN	TR
^{190}At	H. Kokkonen	3/20/2023	17	Jyväskylä	FE
^{189}Lu, ^{191}Hf, ^{192}Hf	K. T. Haak	6/27/2023	18	MSU	PF
^{156}W,[b] ^{160}Os[b]	H. B. Yang	7/5/2023	19	Lanzhou	FE
^{276}Ds, ^{272}Hs, ^{268}Sg	Yu. Ts. Oganessian	7/23/2023	20	Dubna	FE

[a] discovered already in 2022
[b] discovered in 2024, see text

Nuclei at the drip lines and super-heavies

Feature Articles

On the Criteria for Assigning Priority of Discovery of New Elements

Sigurd Hofmann

Pages 14-17 | Published online: 25 Sep 2019

Cite this article https://doi.org/10.1080/10619127.2019.1642705 Check for updates

Abstract

Claiming the discovery of a new element is not sufficient for accepting this claim as a discovery by the scientific community. Careful survey of the presented results is needed to elaborate the correctness of the claim or its rejection in the case of doubtful results.

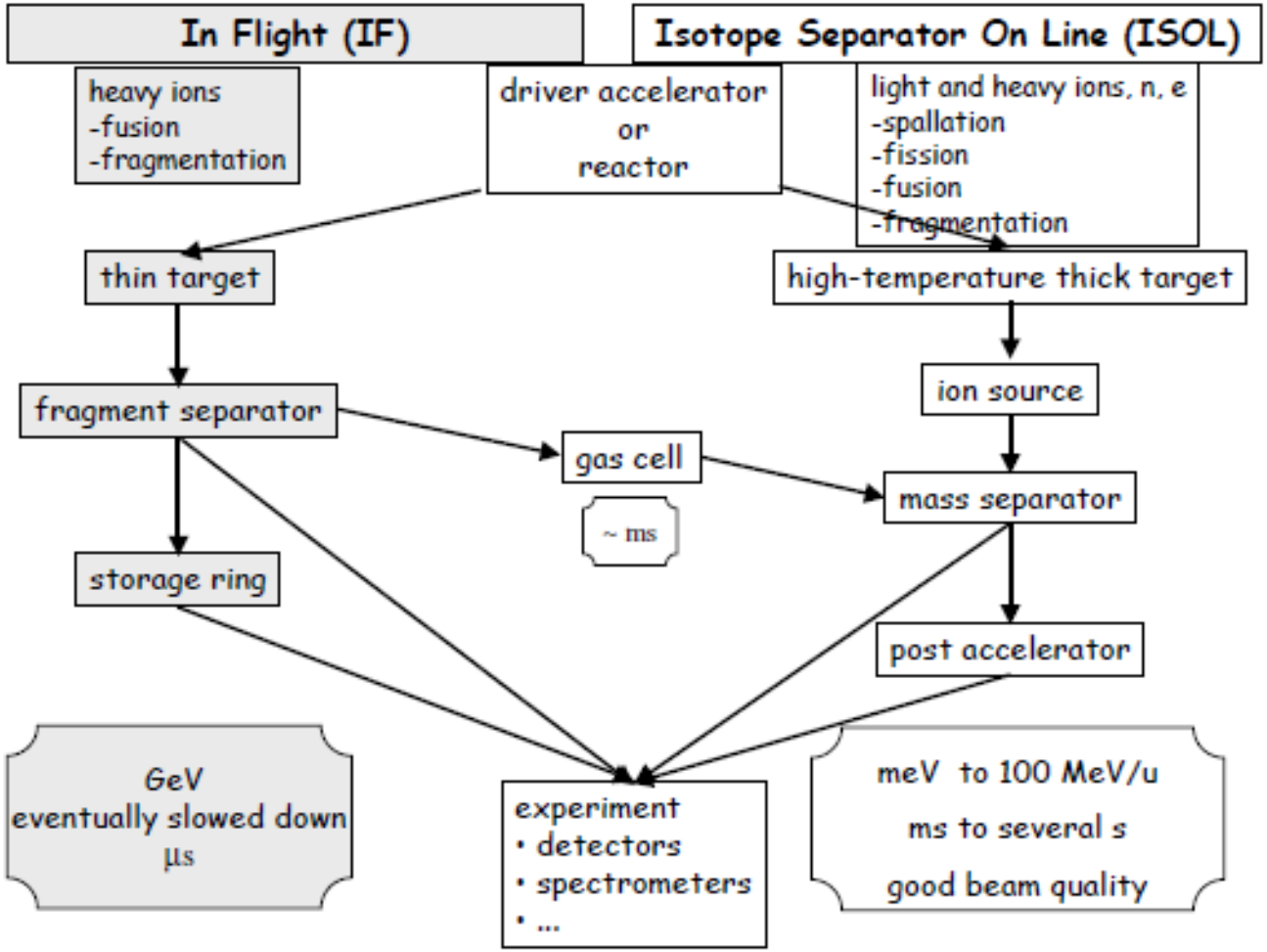

The Why and How of Radioactive-Beam Research

Mark Huyse

University of Leuven, Instituut voor Kern- en Stralingsfysica,
Celestijnenlaan 200 D, 3001 Leuven, Belgium

Measurements of masses and densities of radioactive nuclei

• Masses (or equivalently binding energies) can be measured with good accuracy by means of mass spectrometry.

• The difference between stable and unstable nuclei comes at the level of density measurements. In the case of stable nuclei, electron scattering has been the main source of information. The electromagnetic interaction is known, and this has allowed to interpret the data since the differential elastic cross section for electron scattering is expected to be the Mott cross section (corresponding to the diffusion on a point charge) multiplied by the form factor $F(q^2)$ squared, that is, the Fourier transform of the nuclear charge density,

$$\frac{d\sigma}{d\Omega} = \left(\frac{d\sigma}{d\Omega}\right)_{\text{Mott}} |F(q^2)|^2$$

$$\rho_{\text{charge}}(r) = \frac{1}{2\pi^2 r}\int_0^\infty F(q^2) sin(qr) q dq$$

In the case of unstable nuclei, this is not possible. Sizes and densities have been measured using hadron scattering → with the associated uncertainities !

Chapter 3

SIZES AND ENERGIES OF EXOTIC NUCLEI

3.1 Introduction

The first experiments with unstable nuclear beams were designed to measure the nuclear sizes, namely the matter distribution of protons and neutrons. For stable nuclei such experiments are best accomplished with electron beams, which probe the nuclear charge (proton) distribution. Electron scattering experiments with unstable beams can only be performed in an electron-nucleus collider. Such machines are not yet available. The easiest solution is to measure the *interaction cross section* in collisions of unstable beams with a fixed target nucleus.

The interaction cross section is defined as the cross section for the change of proton and/or neutron number in the incident nucleus. To extract the *interaction radii* of the radioactive secondary beam nuclei, one has assumed that it can be expressed as [1]

$$\sigma_I(P,T) = \pi\,[R_I(P) + R_I(T)]^2 \qquad (3.1)$$

where $R_I(P)$ and $R_I(T)$ are the interaction radii of the projectile and the target nuclei, respectively. $R_I(T)$ can be obtained from σ_I in collisions between identical nuclei, while $R_I(P)$ can be obtained by measuring σ_I for different targets T [1].

The above equation assumes a separability of the projectile and target radius. This hypotheses has been tested by Tanihata and collaborators [1]. As an example, the interaction radii R_I for Li and Be isotopes have been obtained using three different targets. The results are shown in Fig. 1.

In Table 3.1 we show in the first column the interaction radii of several nuclei obtained with this technique [1]. In the last column the root mean charge radius of some nuclei obtained by electron scattering, $R^e_{\rm rms}$, are also shown. One observes that $R^e_{\rm rms}$ is almost constant for $A \geq 6$, while R_I increases with A. One can show that this difference is due to the definitions of the two radii but not due to a difference between the charge and the matter distributions. To prove it we use an eikonal calculation for the cross sections. The *rms* radius of the matter density can be determined independently of the assumed model density functions. The eikonal approximation and its use in nuclear physics is presented in Chapters 1 and 2.

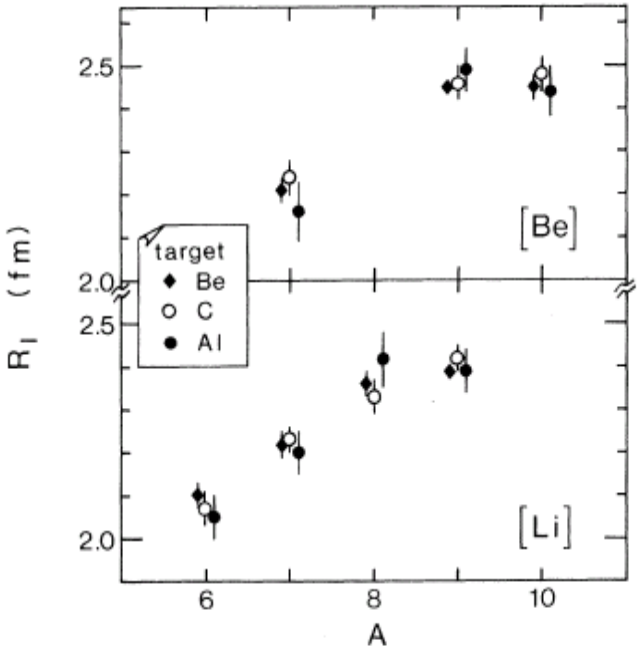

FIG. 1. R_I for Li and Be isotopes. The values obtained by three different targets agree with each other showing the separability of projectile and target R_I.

Table 3.1: cf. next page

TABLE II. Interaction nuclear radii and rms radii, in fermis.

		e scat.	Gaussian	Harmonic oscillator		
	R_I	$R^e_{\rm rms}$	$R^G_{\rm rms}$	$R^m_{\rm rms}$ [a]	$R^c_{\rm rms}$ [a]	$R^n_{\rm rms}$ [a]
^{4}He	1.41 ± 0.03	1.67 ± 0.01	1.72 ± 0.06	1.72 ± 0.06	1.72 ± 0.06	1.72 ± 0.06
^{6}He	2.18 ± 0.02		2.75 ± 0.04	2.73 ± 0.04	2.46 ± 0.04	2.87 ± 0.04
^{8}He	2.48 ± 0.03		2.70 ± 0.03	2.69 ± 0.03	2.33 ± 0.03	2.81 ± 0.03
^{6}Li	2.09 ± 0.02	2.56 ± 0.10	2.54 ± 0.03	2.54 ± 0.03	2.54 ± 0.03	2.54 ± 0.03
^{7}Li	2.23 ± 0.02	2.41 ± 0.10	2.50 ± 0.03	2.50 ± 0.03	2.43 ± 0.03	2.54 ± 0.03
^{8}Li	2.36 ± 0.02		2.51 ± 0.03	2.51 ± 0.03	2.41 ± 0.03	2.57 ± 0.03
^{9}Li	2.41 ± 0.02		2.43 ± 0.02	2.43 ± 0.02	2.30 ± 0.02	2.50 ± 0.02
^{11}Li	3.14 ± 0.16		3.27 ± 0.24	3.27 ± 0.24	3.03 ± 0.24	3.36 ± 0.24
^{7}Be	2.22 ± 0.02		2.48 ± 0.03	2.48 ± 0.03	2.52 ± 0.03	2.41 ± 0.03
^{9}Be	2.45 ± 0.01	2.52 ± 0.01	2.49 ± 0.01	2.50 ± 0.01	2.47 ± 0.01	2.53 ± 0.01
^{10}Be	2.46 ± 0.03		2.38 ± 0.02	2.39 ± 0.02	2.34 ± 0.02	2.43 ± 0.02
^{12}C	2.61 ± 0.02	2.45 ± 0.01	2.40 ± 0.02	2.43 ± 0.02	2.43 ± 0.02	2.43 ± 0.02

[a]Superscripts *m*, *c*, and *n* indicate the nuclear matter, the charge, and the neutron matter distributions, respectively.

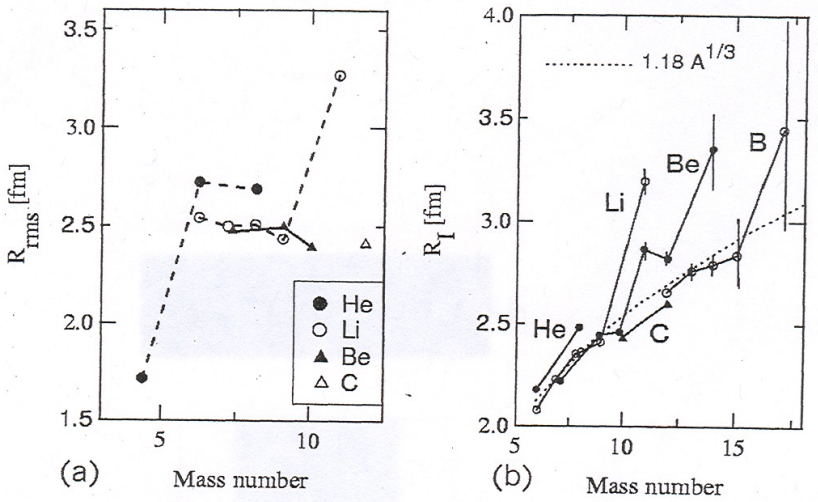

Figure 5 (a) Rms radii for the neutron-rich isotopes He, Li, Be, and C. (b) The matter density radii of several light nuclei compared to the trend $R \sim 1.18\ A^{1/3}$ fm (dashed line) for normal nuclei. The solid lines are guide to the eyes.

The wavefunction of a loosely-bound nucleon (as in the case of the deuteron) extends far beyond the nuclear potential. For large distances the wavefunction behaves as an Yukawa function,

$$R(r)/r \sim \frac{e^{-\eta r}}{r} \tag{3.38}$$

where $(\hbar\eta)^2 = 2mB$, with B equal to the binding energy and m the nucleon mass. Thus, the smaller the value of B is, the more the wavefunction extends to larger $r's$. Thus the "halo" in an exotic unstable nuclei, like ^{11}Li, is a simple manifestation of the weak binding energy of the last nucleons. What is not as trivial is to know why ^{6}He and ^{11}Li are bound while ^{5}He and ^{10}Li are not. We will continue this discussion later.

Abnormally large radii were also found for other light neutron-rich nuclei [7] as shown in figure 5(b).

The matter density radii of these nuclei do not follow the commonly observed trend $R \sim 1.18\ A^{1/3}$ fm of normal nuclei. Thus the halo seems to be a common feature of loosely-bound neutron-rich nuclei. In Table 3.3 we list the spin, parities and mass number of some light neutron-rich nuclei. The separation energy of one neutron (S_n) and of two neutrons (S_{2n}) are also shown. One observes that the two-neutron separation energies of ^{11}Li, ^{14}Be and ^{17}B are very small and are responsible for large matter radii of these nuclei, as seen in figure 5(b). A nuclear chart with the halo nuclei is shown in Figure 6.

Examples: ^{11}Li and ^{11}Be (courtesy: T. Nakamura)

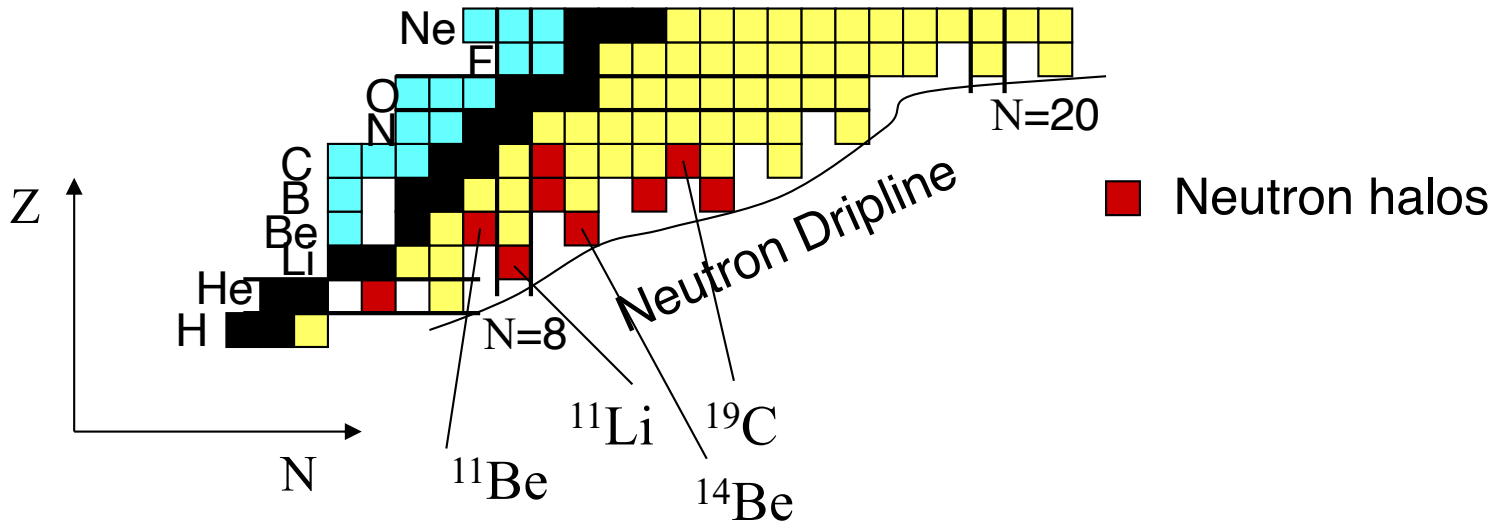

1n halo nucleus

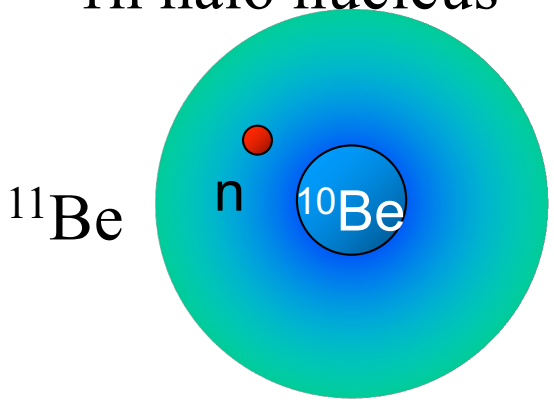

S_n=504 keV

2n halo nucleus

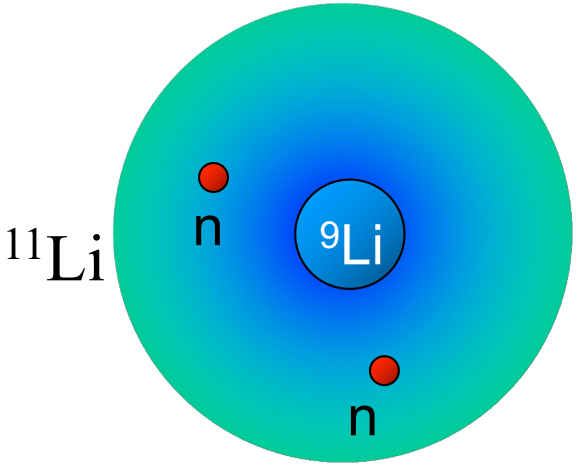

S_{2n}=300 keV

In oder to understand the correlation between the appearance of a halo and the small binding energy of a neutron, we use a simple model (square well). It is well known that in this case, namely

$$V = -V_0 (r < r_0) \qquad = 0 (r > r_0), \qquad (1)$$

the radial Schrödinger equation takes the form

$$-\frac{\hbar^2}{2\mu}\frac{d^2u}{dr^2} + V_{\text{eff}}(r)u = Eu, \qquad (2)$$

where μ is the reduced mass and the effective potential includes the centrifugal term. For ℓ=0, the centrifugal barrier is absent and the solution for negative energy is

$$\begin{aligned} u(r) &= Asin(kr), \quad \text{for } r < r_0 \\ &= Be^{-\eta r}, \quad \text{for } r < r_0, \end{aligned} \qquad (3)$$

where

$$\begin{aligned} k &= \sqrt{\frac{2\mu}{\hbar^2}(V_0 + E)} \\ \eta &= \sqrt{\frac{2\mu|E|}{\hbar^2}}. \end{aligned} \qquad (4)$$

Let us the model (oversimplified !) for the case of ^{11}Be, which is a one-neutron halo.

We know S_n is about 0.5 MeV, so that $\eta \sim 1/6$ fm^{-1}.

The size of the neutron orbit in ^{11}Be is two times the core size

$R_0 A^{1/3} = 2.67$ fm

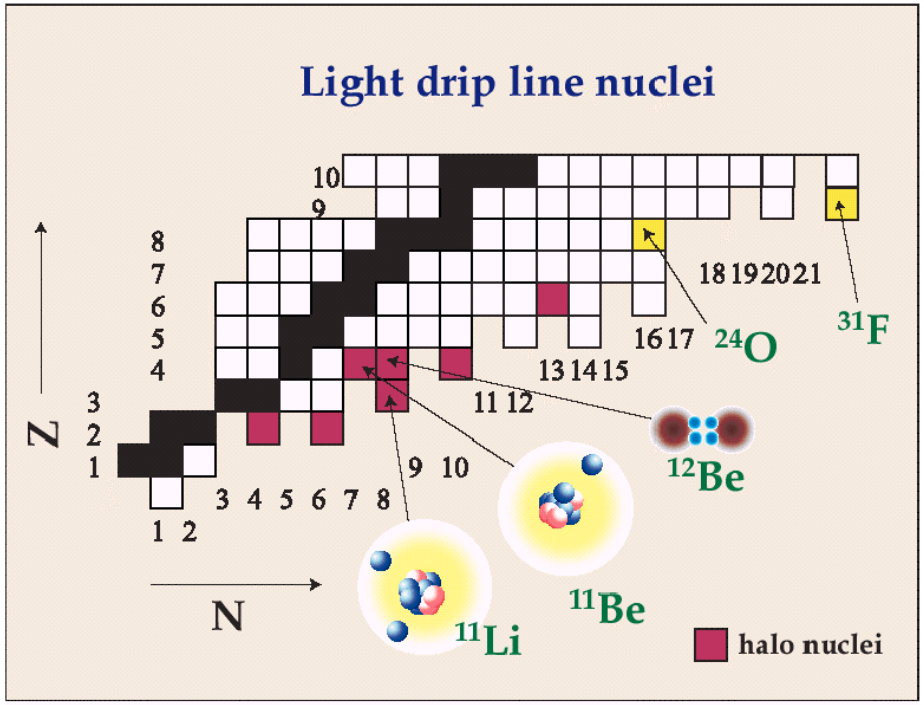

Other evidences

• Other experiments which have been historically important, to make the character of halo nuclei evident, are: (i) momentum distributions of projectile fragments, and (ii) electromagnetic dissociation.

These are reviewed in papers e.g. by I. Tanihata.

The idea of the momentum distribution experiments is quite simple. If we hit, e.g., ^{11}Li on a C target at 800 MeV/u we can measure the transverse momentum of the fragments and we find a “double” distribution.

The component with “small width” has a Δp of about 19 MeV/c. From the uncertainity principle

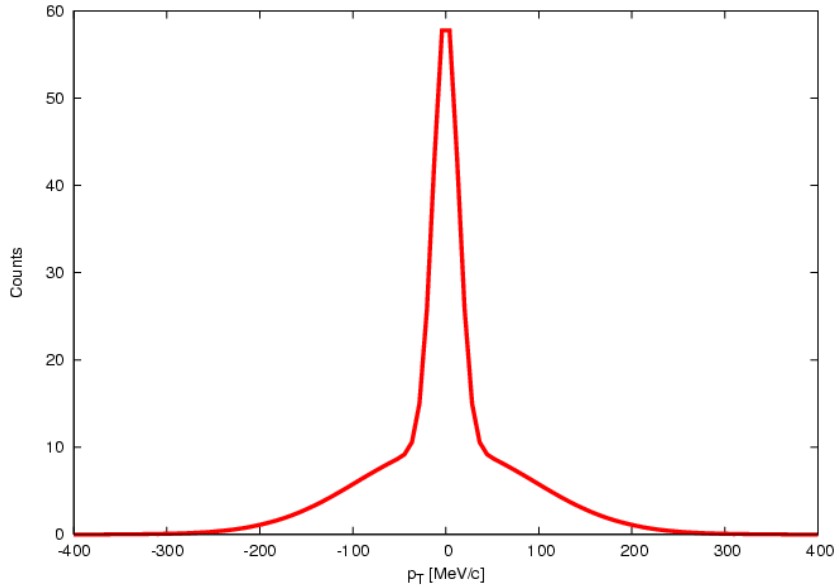

$\Delta x \sim hc/\Delta p \sim 12$ fm,

that is, the narrow component is arising from the halo.